



This is the accepted manuscript made available via CHORUS. The article has been published as:

## Magnetic iron-cobalt silicides discovered using machine-learning

Timothy Liao, Weiyi Xia, Masahiro Sakurai, Renhai Wang, Chao Zhang, Huaijun Sun, Kai-Ming Ho, Cai-Zhuang Wang, and James R. Chelikowsky

Phys. Rev. Materials **7**, 034410 — Published 29 March 2023

DOI: [10.1103/PhysRevMaterials.7.034410](https://doi.org/10.1103/PhysRevMaterials.7.034410)

# Magnetic iron-cobalt silicides discovered using machine-learning

Timothy Liao<sup>1,2</sup>, Weiyi Xia<sup>3,4</sup>, Masahiro Sakurai<sup>1,5</sup>, Renhai Wang<sup>6</sup>, Chao Zhang<sup>7</sup>, Huaijun Sun<sup>8</sup>, Kai-Ming Ho<sup>3</sup>, Cai-Zhuang Wang<sup>3,4,\*</sup> and James R. Chelikowsky<sup>1,2,9,\*</sup>

<sup>1</sup>*Center for Computational Materials, Oden Institute for Computational Engineering and Sciences, The University of Texas at Austin, Austin, Texas 78712, USA*

<sup>2</sup>*Department of Physics, The University of Texas at Austin, Austin, Texas 78712, USA*

<sup>3</sup>*Department of Physics and Astronomy, Iowa State University, Ames, Iowa 50011, USA*

<sup>4</sup>*Ames Laboratory, U.S. Department of Energy, Iowa State University, Ames, Iowa 50011, USA*

<sup>5</sup>*The Institute for Solid State Physics, The University of Tokyo, Kashiwa, Chiba 277-8581, Japan*

<sup>6</sup>*School of Physics and Optoelectronic Engineering, Guangdong University of Technology, Guangzhou 510006, China*

<sup>7</sup>*Department of Physics, Yantai University, Yantai 264005, China*

<sup>8</sup>*Department of Physics, Zhejiang Agriculture and Forestry University, Zhuji 311800, China*

<sup>9</sup>*McKetta Department of Chemical Engineering, The University of Texas at Austin, Austin, Texas 78712, USA*

\* [jrc@utexas.edu](mailto:jrc@utexas.edu), [wangcz@ameslab.gov](mailto:wangcz@ameslab.gov)

## Abstract

We employ machine learning (ML) combined with first principles calculations to discover novel rare-earth-free magnetic iron-cobalt silicide compounds. Deep machine learning models are used to provide rapid screening of over 350,000 hypothetical structures to select a small fraction of promising structures and compositions for further studies by first-principles calculations. Adaptive genetic algorithm (AGA) is used to search for new lower energy structures based on the promising chemical compositions. Such a ML-guided approach dramatically accelerates the pace of materials discovery. We discover four new ternary Fe-Co-Si compounds, which exhibit desirable properties such as a large magnetic polarization ( $J_s > 1.0$  Tesla), a significant easy-axis magnetic anisotropy ( $K_1 \geq 1.0$  MJ/m<sup>3</sup>), and a high Curie temperature ( $T_c > 840$  K). Moreover, the formation energies of these compounds are all within 70 meV/atom relative to the ternary convex hull, offering the possibility of synthesis.

## Introduction

Magnetic materials play an important role in advanced technology and clean energy. Specific applications include computer hard drives, cell phones, medical equipment, electric vehicles, and wind turbines. The key properties governing the performance of a magnet include the magnetization, the magnetocrystalline anisotropy, and the Curie temperature. High anisotropy also allows for high coercivity. Although rare-earth elements could lead to high magnetization and anisotropy, such as the case in  $\text{Nd}_2\text{Fe}_{14}\text{B}_5$  and  $\text{SmCo}_5$ , economic risks call for the search for rare-earth-free alternatives (1-8). Iron-cobalt based compounds in particular appear promising in this respect (9). For example, elemental body-centered cubic Fe and B2-FeCo intermetallics possess sizable ferromagnetic magnetization. However, these compounds are cubic, so no magnetic anisotropy is expected. Anisotropy can be introduced by growing FeCo thin film on substrates, which leads to tetragonal distortion. Alternatively, doping with nonmagnetic elements can stabilize noncubic structures and lead to the enhancement of magnetic anisotropy. Nontoxic dopants for this purpose include Si, N, P, and B. In particular, iron-cobalt silicide is of interest since it is anticipated to be compatible with a silicon substrate. Magnetic devices, such as storage, using this material may be integrated on silicon technology. The subsystems Fe-Si and Co-Si binary phases have been previously studied (10-12). In addition, ternary iron-cobalt silicides of varied levels of crystallinity have been synthesized (13, 14). Most studies on these compounds are focused on characterizing their structural or electric and optical properties. One particular study reported the magnetic properties of two compounds:  $\text{Fe}_2\text{CoSi}$  and  $\text{FeCo}_2\text{Si}$  (15). They possessed sizable magnetization (magnetic moment per metal atom  $> 1.6 \mu\text{B}$ ). However, their in-plane anisotropy (anisotropy constant  $> 1.6 \text{ MJ/m}^3$ ) is not suitable for permanent magnet applications. An extensive exploration of the Fe-Co-Si ternary space to identify easy-axis anisotropy candidates is lacking.

Traditional trial and error with experiment can be inefficient in discovering new materials. Alternatively, data-intensive approaches coupled with first-principles calculations is quickly advancing (8, 16-34). ML can assist in rapidly screening a vast composition space (35-38). The concept of active learning is particularly useful in the context of high throughput first-principles calculations. Active learning seeks to adaptively refine a ML model by expanding the training data in the desired property space. By incorporating new calculated data of relevant structures, the model is expected to improve. Success on using such technique for magnetic materials has been reported for two-dimensional materials (33). However, the size of the dataset was small. A quantitative evaluation of the model improvement is in demand.

We use a ML-guided framework, which we proposed recently (39). Our framework effectively integrates deep neural network ML with first-principles calculations and AGA. We demonstrated the efficiency of this approach in accelerating materials discovery for similar materials – Fe-Co-B. In this paper, we extensively search for new magnetic ternary Fe-Co-Si compounds for permanent magnet applications. The improvement over three “generations” (details below) of models is quantified. We show that training ML on Fe-Co-X data specifically results in an accuracy superior to training on general materials. In addition, feeding back first-principles data of Fe-Co-Si further improves the accuracy. We

discover five new ternary Fe-Co-Si compounds that exhibit high magnetic polarization ( $J_s \geq 1.0$  Tesla), easy-axis magnetic anisotropy ( $K_1 \geq 1.0$  MJ/m<sup>3</sup>), and a high Curie temperature ( $T_c > 840$ K). The formation energies of these compounds are within 70 meV/atom relative to the ternary convex hull. We expect compounds this close to the convex hull to be accessible in terms of synthesis.

## Methods

In our approach, ML models are utilized to provide rapid predictions of chemical compositions and crystal structures, which are likely to be energetically stable and possess desired magnetization. Selected structures from the ML screening are further validated by first-principles calculations, and promising compositions from ML predictions are further explored using AGA to search for low energy structures. Furthermore, new low-energy structures and their properties obtained from the first-principles calculations and AGA search are used to adaptively refine the ML model, thus improving the accuracy of the prediction.

The machine learning model is a crystal graph convolutional neural network (CGCNN) (38). In CGCNN, the crystal structure is represented by a graph. The nodes and the edges represent the atoms and the bonds, respectively. The atomic descriptors include properties such as the location in the periodic table (group and period), the electronegativity, the covalence radius, the number of valence electrons, the first ionization energy, the electron affinity, and the atomic volume. The bond descriptor is the bond length. Convolutional layers “convolutes” the atom feature vectors with their neighboring atoms and bonds. A pooling layer sums the atom feature vectors into one overall feature vector. After a few hidden layers, the prediction is output. The depths mentioned are optimized. In this study, we set the hyperparameters mostly to default values in the code provided in Ref. 38. We use 3 convolutional layers, one pooling layer, and one hidden layer after pooling for the model training. Batch size is set to 256 and total number of epochs to run is set to 100. Stochastic Gradient Descent is used as optimization algorithm. Crystal structures and their properties are the input to the training (and validation and testing) of the model. When a collection of new structures without the correspond properties are supplied, the ML model outputs the predicted properties. After 100 epochs of run, the best model with the minimum mean absolute error of the validation set is selected. Mean absolute error here is used as the criteria of the accuracy of the prediction, which is adaptively improved through an iterative process. The first CGCNN model was directly adopted from Ref. 38, which was trained using the structures and energies of 28,046 compounds in the Materials Project database from density functional theory (DFT) calculations (38). We refer to this model as the first generation (1G) generalized CGCNN model. In training the models, the dataset is divided into training set (80%), validation set (10%) and test set (10%). The mean absolute error of the validation set for the 1G model for formation energy is 0.039 eV/atom. 1G-CGCNN is used to screen hypothetical structures. Then a second generation (2G) CGCNN model is trained using the DFT formation energies of 427 Fe-Co-Si structures selected from the prediction of 1G-CGCNN and 3469 Fe-Co-X (X=B, C, N, S) structures from our novel magnetic materials database (8). Finally, a third generation (3G) CGCNN model is

further trained by adding 1775 Fe-Co-Si structures from 2G-CGCNN prediction and AGA structure search (details below).

The trained 2G-CGCNN for formation energy prediction has low mean absolute error for the validation set (0.104 eV/atom) and the test set (0.136 eV/atom). 3G-CGCNN has lower mean absolute error for validation set (0.058 eV/atom) and test set (0.60 eV/atom). We note that 1G-CGCNN is more general since it is trained on data involving many different combinations of chemical elements. On the other hand, the 2G and 3G-CGCNN models are specifically trained on Fe-Co-X systems. For magnetic polarization, we use the same procedure as above.

The first-principles calculations are based on DFT (40). We adopt the generalized gradient approximation of Perdew, Burke, and Ernzerhof (PBE) (41) for the exchange-correlation energy functional. We selected the projector-augmented wave (PAW) method (42). The Monkhorst-Pack scheme (43) is utilized to generate a  $k$ -point grid with a mesh size of  $2\pi \times 0.025 \text{ \AA}^{-1}$  for spin-polarized calculations (44). A cutoff energy of at least 500 eV is used for the wavefunctions. These settings are used to compute the formation energy and magnetization of structures from ML and AGA (45).

We employ AGA to search for low energy structures for a given chemical composition (46, 47). For each composition, up to four formula units per unit cell are generated with initial 128 randomized structures. AGA adds an additional loop on the traditional GA loop to adaptively adjust the interatomic potential. The most time-consuming step of structural optimization and energy evaluation is accelerated by using an auxiliary interatomic potential based on the embedded atom method (48). One-shot DFT calculations are performed at the end of each GA cycle on several of the lowest energy structures. The DFT results are used to update the parameters of the potential. Another cycle of GA search is then performed using the latest adjusted interatomic potential. This is followed by a re-adjustment of the potential parameters. The AGA iteration process is then repeated. AGA enjoys the efficiency of the traditional GA prediction while retaining a high level of accuracy owing to the DFT feedback.

The formation energy per atom relative to the elemental phases of a  $\text{Fe}_\alpha\text{Co}_\beta\text{Si}_\gamma$  with  $\alpha+\beta+\gamma=1$  is defined as

$$E_f = E(\text{Fe}_\alpha\text{Co}_\beta\text{Si}_\gamma) - \alpha E(\text{Fe}) - \beta E(\text{Co}) - \gamma E(\text{Si}).$$

Here,  $E(\text{Fe}_\alpha\text{Co}_\beta\text{Si}_\gamma)$  is the total energy per atom of a  $\text{Fe}_\alpha\text{Co}_\beta\text{Si}_\gamma$  structure. Reference energies are the total energies per atom of body-centered cubic Fe, hexagonal close-packed Co, and diamond Si. We also calculate the energy above convex hull,  $E_{hull}$ , by comparing the formation energy of  $\text{Fe}_\alpha\text{Co}_\beta\text{Si}_\gamma$  with respect to the nearby three known stable phases. The chemical compositions of these phases are located at the vertexes of the Gibbs triangle that encloses the composition of  $\text{Fe}_\alpha\text{Co}_\beta\text{Si}_\gamma$ . We use this construction to assess the thermodynamic stability against decomposition into the stable phases.

We calculate the magnetocrystalline anisotropy energy for the structures with high magnetic polarization ( $J_s > 1.0$  Tesla) and with formation energies within 0.1 eV/atom above the convex hull. We perform spin-polarized calculations for collinear magnetism self-consistently. We then include the spin-orbit couplings and perform a non-self-consistent calculation (49-51). When the spin-orbit couplings are included, symmetry operations are removed and the spin-quantization axis is set to the chosen direction. For the magnetocrystalline anisotropy calculations, we use a finer mesh size of  $2\pi \times 0.016 \text{ \AA}^{-1}$  to achieve better accuracy. For the candidate structures, the formation energy and magnetization are updated using these settings.

For each structure, we calculate the total energy for magnetic moments oriented along the Cartesian (100), (010), and (001) directions, respectively. The direction associated with the lowest total energy is labeled as the magnetic “easy” direction. The direction with the second lowest total energy is labeled as the “intermediate” direction. The magnetocrystalline anisotropy constants  $K_1$  is the total-energy difference between the ferromagnetic states with magnetization in the easy and intermediate directions divided by the unit cell volume:

$$K_1 = (E_{intermediate} - E_{easy})/V$$

A high easy-axis anisotropy is desirable for permanent magnet applications.

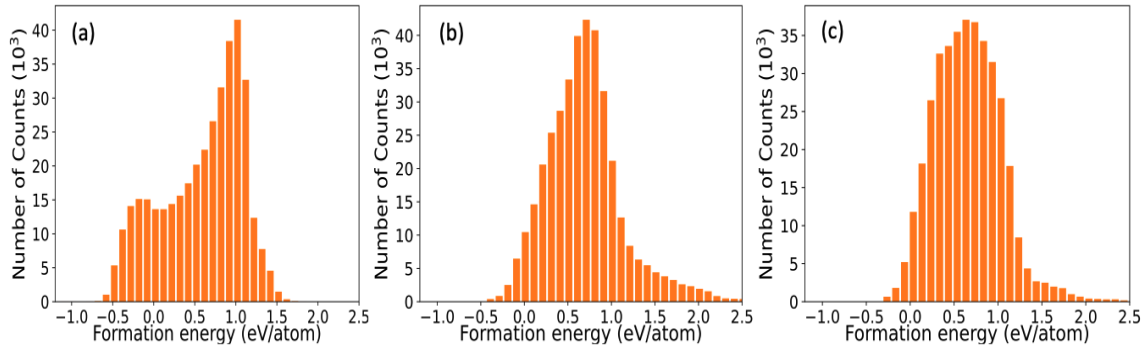
We calculate Curie temperature  $T_c$  using a full potential Korringa-Kohn-Rostocker (KKR) Green function method (52, 53). The non-spherical part of the potential is taken into account in the wavefunctions exactly. The method has advantages of speed, accuracy, and stability.

The phonon dispersion is calculated using density functional perturbation theory through the Phonopy code (54, 55).

## Results and Discussion

We first collect the 11,916 ternary structures from MP which all have an experimental ID in the Inorganic Crystal Structure Database (ICSD) (56). A structure pool of hypothetical ternary Fe-Co-Si compounds is then generated by threading the three elements Fe, Co, and Si on the lattice of the 11,916 structures. There are six ways to shuffle the three elements on a ternary structure. We also allow the volume of the unit cell to vary by a scaling factor of 0.96 to 1.04, in increments of 0.02. Since the CGCNN model does not have the interatomic forces to relax the bond lengths in the structures, the use of scaling factor for the volume helps the model differentiate the energetic stability of the same structure with different bond lengths. There are 357,480 ternary Fe-Co-Si structures generated in this way. The 1G-CGCNN model is first used to evaluate the formation energy of these 357,480 structures. The model predicted that there are 832 structures having  $E_f < -0.5$  eV/atom. We show the distribution in **Fig. 1 (a)**. Out of these, 427 were found to have negative formation energy after DFT structural optimization and removing equivalent structures.

**Fig. 1: Formation energy distribution from ML predictions**



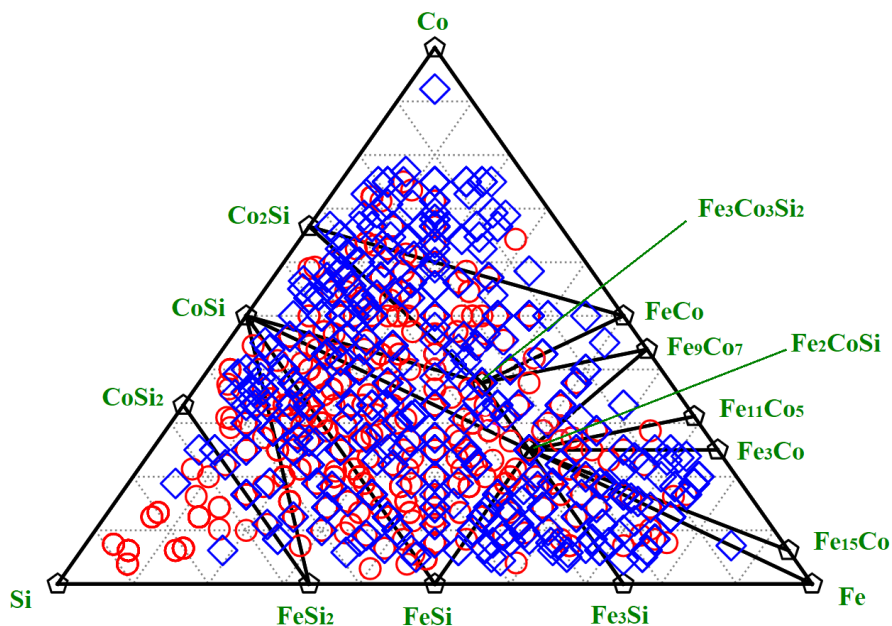
Formation energies from the (a) first, (b) second, (c) and third generations CGCNN models for structures generated from the MP database. The total number of structures are 357,480 in (a) and (b) and 854,070 in (c).

We also apply the 2G-CGCNN on the 357,480 hypothetical structures. The formation energy distribution is shown in **Fig. 1 (b)**. Structures with negative predicted  $E_f$  are selected for DFT optimization, after which 4,014 non-equivalent new structures are found to have negative  $E_f$ .

Next, we apply the 3G-CGCNN to a larger hypothetical structure pool. The pool is generated in the same way as described above except we collect all ternary structures from MP including those without an experimental ID in ICSD to access more structures. There are 854,070 hypothetical Fe-Co-Si structures in this larger pool. The formation energy histogram from 3G-CGCNN prediction is shown in **Fig. 1 (c)**. There are 6,185 non-equivalent new structures with predicted  $E_f < 0$  eV. By further applying the ML model for magnetization prediction (35), we find that only 4,748 are predicted to have  $J_s > 0.5$  Tesla. These 4,748 structures are optimized by DFT calculations, resulting in 1,119 non-equivalent structures which cover 270 compositions. The distribution of these 270 compositions and those obtained from DFT calculations on the 1G and 2G-CGCNN selected structures are shown in **Fig. 2**.

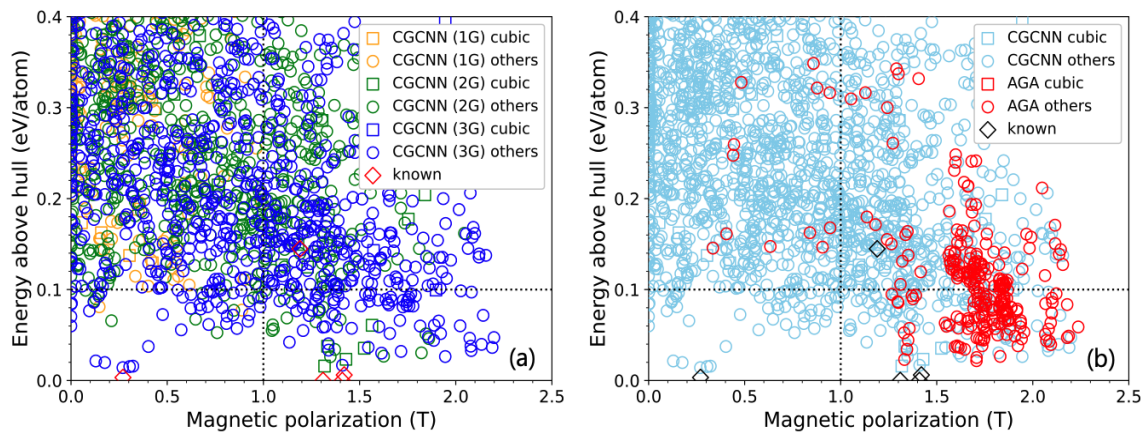
In **Fig. 3 (a)**, the energetic stability and magnetic polarization from DFT calculation for the structures selected by different ML generations are displayed. Structures with  $E_{hull} < 0.1$  eV/atom and  $J_s > 1$  Tesla would be promising for magnetic materials. We can see that there are no structures from 1G-CGCNN selection in this area. The structures with  $E_{hull} < 0.1$  eV/atom and  $J_s > 2$  Tesla all come from 3G and are non-cubic.

**Fig. 2: Convex hull phase diagram.**



Known stable phases on the convex hull are indicated by black pentagons. Compositions examined by ML are labeled with red circles indicating those examined by 1G+2G and blue diamonds by 3G.

**Fig. 3: Stability and magnetic polarization**

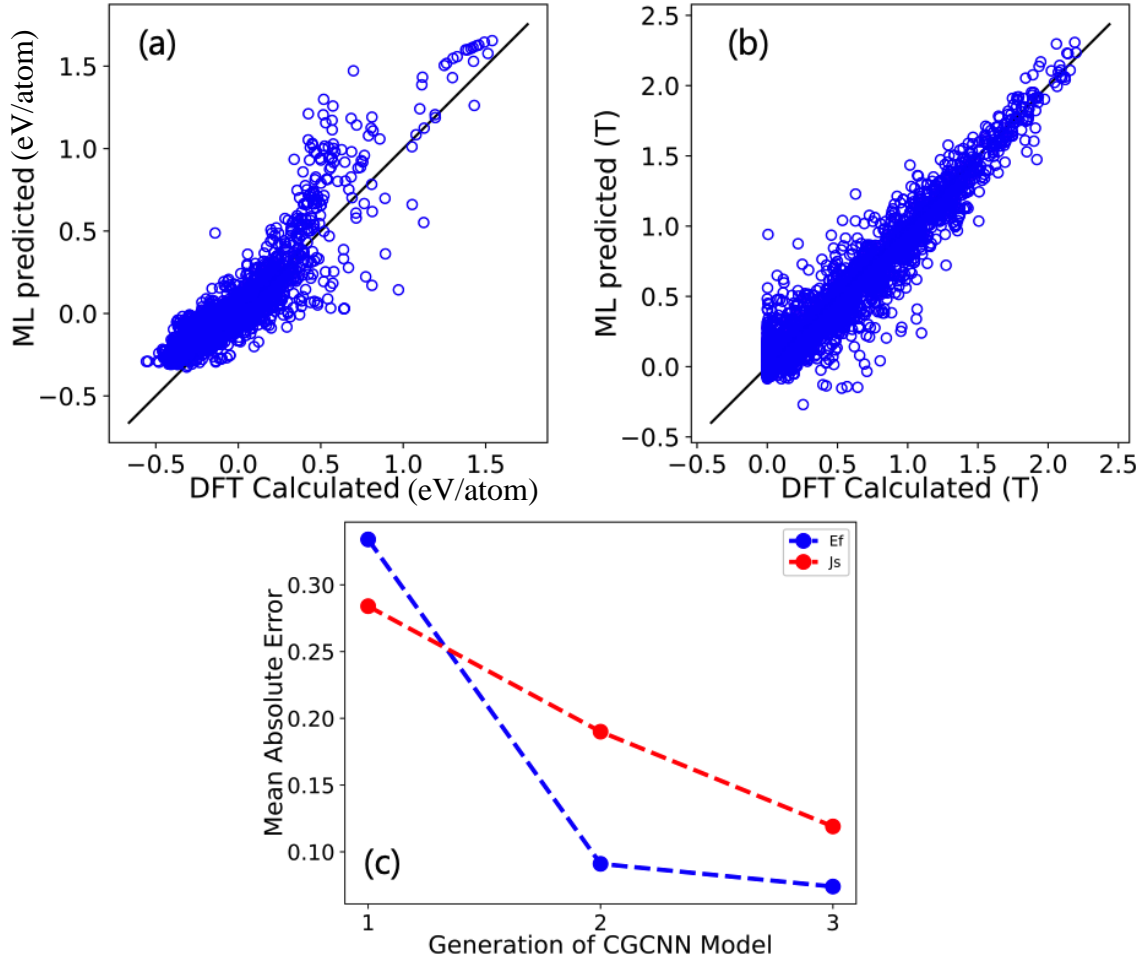


Stability and magnetic polarization of structures from (a) ML (b) and AGA compared to ML. Diamond markers indicate known structures from MP.

From the ML screening and DFT calculation, we discover 8 promising compositions which are transition-metal rich and yields low-energy and high-magnetization structures. The compositions are Fe-Co-Si = 2-1-1, 4-5-1, 12-1-3, 3-4-1, 9-1-2, 9-2-1, 15-4-1, and 6-1-1. These compositions are chosen for further exploration by AGA. 40 AGA iterations are performed, with 16 candidate structures selected from each iteration. After 40 AGA iterations, 50 structures are selected with the lowest energies calculated by DFT. We get 1,000 structures from AGA search in total. In **Fig. 3 (b)**, the formation energy and magnetic polarization for the structures from AGA are compared to those from ML. We can see that a large proportion of AGA structures are within the “target region”:  $E_{hull} < 0.1$  eV/atom,  $J_s > 1$  Tesla and are non-cubic. For Fe-Co-Si compositions of 9-1-2 and 6-1-1, some structures obtained from AGA are energetically more favorable than those obtained by CGCNN screening.

To demonstrate how the iterative process can effectively improve the accuracy of the CGCNN model for the system of interest, we examine the accuracy of different generations of the model on 2,281 Fe-Co-Si new structures obtained by our CGCNN and AGA search. The prediction accuracy of 2G improves upon 1G because 2G is specifically trained on Fe-Co-X structures. Then the model is being further optimized by feeding in more Fe-Co-Si to the 3G-CGCNN training. In **Fig. 4 (a)** and **(b)**, we see that  $E_f$  and  $J_s$  of Fe-Co-Si structures predicted by the 3G model are in good agreement with those from DFT calculations. The mean absolute error for predicting  $E_f$  evolves from 0.334 eV/atom for 1G, 0.091 eV/atom for 2G, to 0.082 eV/atom for 3G as shown in **Fig. 4 (c)**. Similarly, 0.284, 0.190, 0.119 Tesla for 1G, 2G, 3G for  $J_s$  prediction. The improvement of  $E_f$  prediction from 1G to 2G is especially significant compared to that from 2G to 3G. The  $J_s$  prediction improves at a roughly constant rate over the generations.

**Fig. 4: ML predictions for  $E_f$  and  $J_s$  compared to DFT results.**



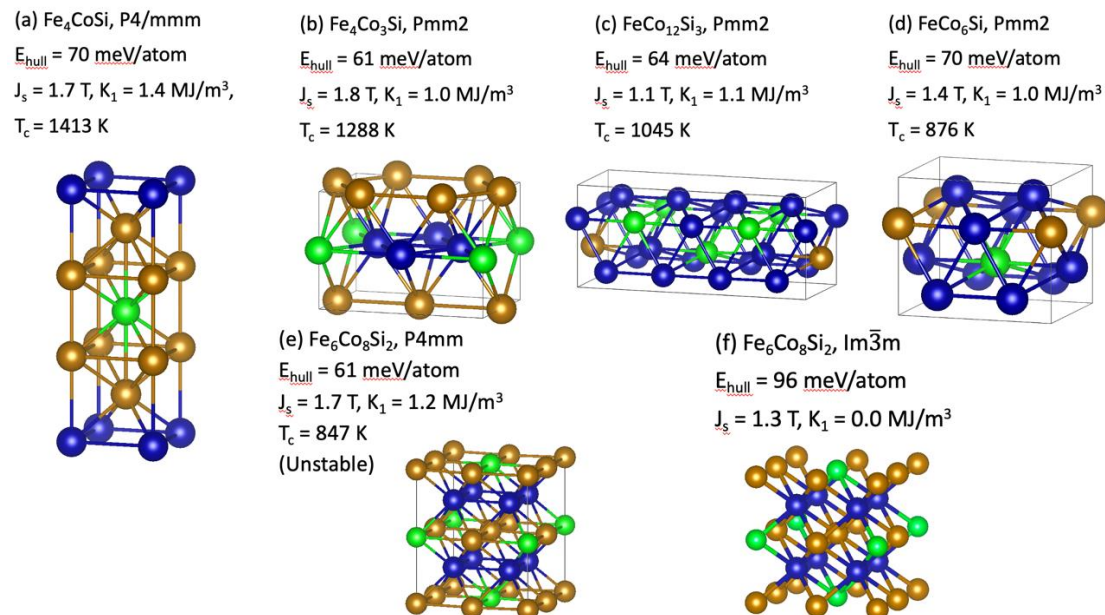
(a) Formation energies,  $E_f$ , and (b) magnetic polarization,  $J_s$ , of Fe-Co-Si structures predicted by 3G-CGCNN model compared to DFT calculations. (c) Evolution of the ML model over generations. Mean absolute errors in predicting  $E_f$  and  $J_s$  are shown in blue and red, respectively.

According to **Fig. 3 (b)**, we obtained 114 structures from our CGCNN+DFT+AGA approach with  $E_{hull} < 0.1$  eV/atom and  $J_s > 1$  Tesla. We evaluate the magnetic anisotropy constant  $K_1$  and Curie temperature  $T_c$  for these 114 structures using DFT calculations. We found five structures with  $K_1 \geq 1$  MJ/m<sup>3</sup> and  $T_c$  higher than 840 K. Their formation energies are within 70 meV/atom above the convex hull. We carried out the phonon calculations for the 5 structures shown in **Fig. 5 (a)-(e)**. Four ( **(a)-(d)** ) of these structures are found to be dynamically stable. The Fe<sub>6</sub>Co<sub>8</sub>Si<sub>2</sub> structures shown in **Fig. 5 (e)** exhibits some imaginary modes. We attempted to stabilize this structure by moving the atoms in the direction of the eigenvector of the soft phonon mode near R then relaxing the structure. We arrived at a dynamically stable structure with lower energy as shown in **Fig. 5 (f)**. However, this lower-energy and dynamically stable structure is a cubic structure and has no magnetic

anisotropy. Further investigation by inserting small elements (e.g., B or N) into the interstitial sites to stabilize the structure in the tetragonal symmetry to enhance and magnetic anisotropy might be interesting. We present the phonon dispersion in **Fig. 6**. One candidate structure in **Fig. 5 (a)** resembles a stacking of body-centered cells. The other three candidate structures in **Fig. 5 (b), (c), and (d)** are in the  $Pmm2$  space group. Among these,  $\text{Fe}_4\text{CoSi}$  with space group  $P4/mmm$  has large  $J_s = 1.7$  T,  $K_1 = 1.4$  MJ/m<sup>3</sup> and the highest  $T_c = 1,413$  K. More structure information on these four promising ternary compounds is given in the Supplementary Material (57).

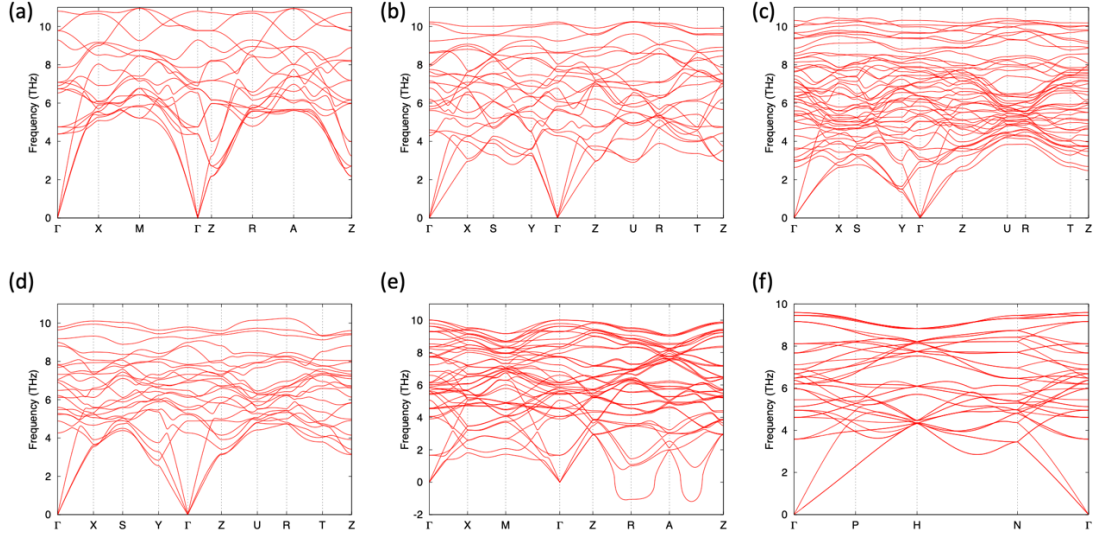
Finally, we confirm that ferromagnetic (FM) configuration is indeed the ground state for the candidates. We test a number of antiferromagnetic (AFM) configurations of the four final candidates. We check configurations in which the spins of each metal layer point in the same direction (detailed figures are in the Supplementary Material (57)). Inter-layer directions point oppositely. For our top candidate,  $\text{Fe}_4\text{CoSi}$ , we also extensively examine 27 AFM configurations, including 1x2x1 supercells. The FM configuration is found to be lower in energy than all of the AFM configurations by at least 43 meV/atom. These results confirm that the four candidates are promising for permanent magnet applications. In magnetic materials studies, the stability comparison of FM/AFM is important. ML models to study FM/AFM competitions would be interesting but also more challenging (see, for example, Ref. 33). However, since the scope of this paper is to find stable FM structures for rare-earth free permanent magnets, ML models trained for FM structure predictions are a more efficient approach. As long as the predicted FM structures (usually small numbers for a given ternary) are checked to be energetically favorable than the competing AFM states by ab initio calculations, "false positive" FM predictions can be avoided. Those structures which have AFM as ground state would likely be eliminated by such ML screenings, but these structures are not suitable for permanent magnets and are not what we are searching for in this paper.

**Fig. 5: Candidate structures with easy-axis anisotropy.**



Fe, Co, and Si atoms are indicated by yellow, blue and green spheres, respectively. (a) – (d) are the four candidate structures. (e) stabilizes to (f), which has no anisotropy.

**Fig. 6: Phonon dispersion of the candidate structures.**



Phonon dispersion corresponding to **Fig. 5**.

## Summary

Iron-cobalt silicides are promising rare-earth-free magnet candidates since they may be integrated with silicon technology. We utilized a machine learning guided framework with first principles calculations to discover such ternary compounds. Three generations of CGCNN ML models screened more than 350,000 theoretical structures. AGA was useful for access to new low energy structures based on the promising compositions selected by ML. We demonstrated that the accuracy of the ML models can be improved adaptively by incorporating additional Fe-Co-Si structures obtained from the ML and AGA search in the training dataset. We proposed four easy-axis anisotropy candidates for synthesis. In particular, the easy-axis  $\text{Fe}_4\text{CoSi}$  compound possessed  $J_s = 1.7$  Tesla,  $K_1 = 1.4$  MJ/m<sup>3</sup>,  $T_c = 1,413$  K.

## Data availability

The data leading to the findings in this paper are available on Materials Project (24) and Magnetic Materials Database (8). The ML models are available from the authors upon reasonable request.

## Acknowledgments

The application of the ML-guided framework and AGA to the discovery of the Fe-Co-Si ternary magnetic compounds was supported by the U.S. National Science Foundation (NSF) through the Designing Materials to Revolutionize and Engineer our Future (DMREF) program with the award numbers of 1729202 and 1729677. The development of the ML-guided framework and AGA method was supported by the U.S. Department of Energy (DOE), Office of Science, Basic Energy Sciences, Materials Science and Engineering Division under contract # DE-AC02-07CH11358, including the computer time allocation at the National Energy Research Scientific Computing Center (NERSC) in Berkeley, California. High performance computing resources were also provided by the Texas Advanced Computing Center (TACC), through the Extreme Science and Engineering Discovery Environment (XSEDE) allocation, and by the Supercomputer Center at the Institute for Solid State Physics (ISSP), the University of Tokyo.

## References

1. J. M. D. Coey, H. Sun, Improved magnetic properties by treatment of iron-based rare earth intermetallic compounds in ammonia. *J. Magn. Magn. Mater.* **87**, L251-L254 (1990).
2. J. F. Herbst, R<sub>2</sub>Fe<sub>14</sub>B materials: Intrinsic properties and technological aspects. *Rev. Mod. Phys.* **63**, 819-898 (1991).
3. J. M. D. Coey, Magnetism and Magnetic Materials. (Cambridge University Press, 2010).
4. T. Miyake, K. Terakura, Y. Harashima, H. Kino, S. Ishibashi, First-Principles Study of Magnetocrystalline Anisotropy and Magnetization in NdFe<sub>12</sub>, NdFe<sub>11</sub>Ti, and NdFe<sub>11</sub>TiN. *J. Phys. Soc. Jpn.* **83**, 043702 (2014).
5. T. Miyake, H. Akai, Quantum Theory of Rare-Earth Magnets. *J. Phys. Soc. Jpn.* **87**, 041009 (2018).
6. J. Cui, M. Kramer, L. Zhou, F. Liu, A. Gabay, G. Hadjipanayis, B. Balasubramanian, D. Sellmyer, Current progress and future challenges in rare-earth-free permanent magnets. *Acta Mater.* **158**, 118-137 (2018).
7. B. Balasubramanian, M. Sakurai, C.-Z. Wang, X. Xu, K.-M. Ho, J. R. Chelikowsky, D. J. Sellmyer, Synergistic computational and experimental discovery of novel magnetic materials. *Mol. Syst. Des. Eng.* **5**, 1098-1117 (2020).
8. M. Sakurai, R. Wang, T. Liao, C. Zhang, H. Sun, Y. Sun, H. Wang, Xin Zhao, S. Wang, B. Balasubramanian, X. Xu, D. J. Sellmyer, V. Antropov, J. Zhang, C.-Z. Wang, K.-M. Ho, J. R. Chelikowsky, Discovering rare-earth-free magnetic materials through the development of a database. *Phys. Rev. Mater.* **4**, 114408 (2020).
9. A. G. Kusne, T. Gao, A. Mehta, L. Ke, M. C. Nguyen, K.-M. Ho, V. Antropov, C.-Z. Wang, M. J. Kramer, C. Long, I. Takeuchi, On-the-fly machine-learning for high-throughput experiments: search for rare-earth-free permanent magnets. *Sci. Rep.* **4**, 6367 (2014).
10. B. Balasubramanian, P. Manchanda, R. Skomski, P. Mukherjee, S. R. Valloppilly,

- B. Das, G. C. Hadjipanayis, D. J. Sellmyer, High-coercivity magnetism in nanostructures with strong easy-plane anisotropy. *Appl. Phys. Lett.* **108**, 152406 (2016).
11. X. Zhao, S. Yu, S. Wu, M. C. Nguyen, C.-Z. Wang, K.-M. Ho, Structures, phase transitions, and magnetic properties of Co<sub>3</sub>Si from first-principles calculations. *Phys. Rev. B* **96**, 024422 (2017).
  12. Z. Yang, S. Wu, X. Zhao, M. C. Nguyen, S. Yu, T. Wen, L. Tang, F. Li, K.-M. Ho, C.-Z. Wang, Structures and magnetic properties of iron silicide from adaptive genetic algorithm and first-principles calculations. *J. Appl. Phys.* **124**, 073901 (2018).
  13. G. A. Landrum, R. Hoffmann, J. Evers, H. Boysen, The TiNiSi Family of Compounds: Structure and Bonding. *Inorg. Chem.* **37**, 5754-5763 (1998).
  14. G. V. Raynor, V. G. Rivlin, 18: Critical evaluation of constitution of cobalt-iron-silicon and iron-nickel-silicon alloys. *Int. Met. Rev.* **30**, 181-210 (1985).
  15. D. Berling, P. Bertoncini, M.C. Hanf, A. Mehdaoui, C. Pirri, P. Wetzel, G. Gewinner, B. Loegel, Magnetic properties in epitaxial binary iron and ternary iron-cobalt silicide thin films grown on Si (111). *J. Magn. Magn. Mater.* **212**, 323-336 (2000).
  16. J. E. Saal, S. Kirklin, M. Aykol, B. Meredig, C. Wolverton, Materials Design and Discovery with High-Throughput Density Functional Theory: The Open Quantum Materials Database (OQMD). *JOM* **65**, 1501-1509 (2013).
  17. G. R. Schleder, A. C. M. Padilha, C. M. Acosta, M. Costa, A. Fazzio, From DFT to machine learning: recent approaches to materials science—a review. *Journal of Physics: Materials* **2**, 032001 (2019).
  18. L. Himanen, A. Geurts, A. S. Foster, P. Rinke, Data-Driven Materials Science: Status, Challenges, and Perspectives. *Adv. Sci.* **6**, 1900808 (2019).
  19. S. Curtarolo, W. Setyawan, G. L.W. Hart, M. Jahnatek, R. V. Chepulskii, R. H. Taylor, S. Wang, J. Xue, K. Yang, O. Levy, *et al.*, AFLOW: An automatic framework for high-throughput materials discovery. *Comput. Mater. Sci.* **58**, 218-226 (2012).
  20. J. Cai, X. Chu, K. Xu, H. Li, J. Wei, Machine learning-driven new material discovery. *Nanoscale Adv.* **2**, 3115-3130 (2020).
  21. K. T. Butler, D. W. Davies, H. Cartwright, O. Isayev, A. Walsh, Machine learning for molecular and materials science. *Nature* **559**, 547-555 (2018).
  22. J. E. Gubernatis, T. Lookman, Machine learning in materials design and discovery: Examples from the present and suggestions for the future. *Phys. Rev. Mater.* **2**, 120301 (2018).
  23. R. Vasudevan, G. Pilania, P. V. Balachandran, Machine learning for materials design and discovery. *J. Appl. Phys.* **129**, 070401 (2021).
  24. A. Jain, S. P. Ong, G. Hautier, W. Chen, W. D. Richards, S. Dacek, S. Cholia, D. Gunter, D. Skinner, G. Ceder, K. A. Persson, Commentary: The Materials Project: A materials genome approach to accelerating materials innovation. *APL Mater.* **1**, 011002 (2013).
  25. C. Draxl, M. Scheffler, The NOMAD laboratory: from data sharing to artificial intelligence. *J. Phys. Mater.* **2**, 036001 (2019).
  26. S. Sanvito, C. Oses, J. Xue, A. Tiwari, M. Zic, T. Archer, P. Tozman, M.

- Venkatesan, M. Coey, S. Curtarolo, Accelerated discovery of new magnets in the Heusler alloy family. *Sci. Adv.* **3** (2017).
27. P. Nieves, S. Arapan, J. Maudes, R. Marticorena, N.L. Del Brío, A. Kovacs, C. Echevarria-Bonet, D. Salazar, J. Weischenberg, H. Zhang, *et al.*, Database of novel magnetic materials for high-performance permanent magnet development. *Comput. Mater. Sci.* **168**, 188-202 (2019).
  28. A. Kabiraj, M. Kumar, S. Mahapatra, High-throughput discovery of high Curie point two-dimensional ferromagnetic materials. *NPJ Comput. Mater.* **6**, 35 (2020).
  29. D. Torelli, H. Moustafa, K. W. Jacobsen, T. Olsen, High-throughput computational screening for two-dimensional magnetic materials based on experimental databases of three-dimensional compounds. *NPJ Comput. Mater.* **6**, 158 (2020).
  30. H. Zhang, High-throughput design of magnetic materials. *Electron. Struct.* **3**, 033001 (2021).
  31. G. A. Landrum, H. Genin, Application of machine-learning methods to solid-state chemistry: ferromagnetism in transition metal alloys. *J. Solid State Chem.* **176**, 587-593 (2003).
  32. I. Miyazato, Y. Tanaka, K. Takahashi, Accelerating the discovery of hidden two-dimensional magnets using machine learning and first principle calculations. *J. Phys. Condens. Matter.* **30**, 06LT01 (2018).
  33. T. D. Rhone, W. Chen, S. Desai, S. B. Torrisi, D. T. Larson, A. Yacoby, E. Kaxiras, Data-driven studies of magnetic two-dimensional materials. *Sci. Rep.* **10**, 15795 (2020).
  34. Y. Xie, G. A. Tritsarlis, O. Grånäs, T. D. Rhone, Data-Driven Studies of the Magnetic Anisotropy of Two-Dimensional Magnetic Materials. *J. Phys. Chem. Lett.* **12**, 12048-12054 (2021).
  35. T. Liao, W. Xia, M. Sakurai, R. Wang, C. Zhang, H. Sun, K.-M. Ho, C.-Z. Wang, J. R. Chelikowsky, Predicting magnetic anisotropy energies using site-specific spin-orbit coupling energies and machine learning: Application to iron-cobalt nitrides. *Phys. Rev. Mater.* **6**, 024402 (2022).
  36. J. Nelson, S. Sanvito, Predicting the Curie temperature of ferromagnets using machine learning. *Phys. Rev. Mater.* **3**, 104405 (2019).
  37. A. Dutta, P. Sen, Machine learning assisted hierarchical filtering: a strategy for designing magnets with large moment and anisotropy energy. *J. Mater. Chem. C* **10**, 3404-3417 (2022).
  38. T. Xie, J. C. Grossman, Crystal Graph Convolutional Neural Networks for an Accurate and Interpretable Prediction of Material Properties. *Phys. Rev. Lett.* **120**, 145301 (2018).
  39. W. Xia, M. Sakurai, B. Balasubramanian, T. Liao, R. Wang, C. Zhang, H. Sun, K.-M. Ho, J. R. Chelikowsky, D. J. Sellmyer, C.-Z. Wang, Accelerating the discovery of novel magnetic materials using machine learning-guided adaptive feedback. *Proc. Natl. Acad. Sci. U.S.A* **119** (47) e2204485119 (2022).
  40. W. Kohn, L. J. Sham, Self-Consistent Equations Including Exchange and Correlation Effects. *Phys. Rev.* **140**, A1133-A1138 (1965).
  41. J. P. Perdew, K. Burke, M. Ernzerhof, Generalized Gradient Approximation Made Simple. *Phys. Rev. Lett.* **77**, 3865-3868 (1996).
  42. P. E. Blöchl, Projector augmented-wave method. *Phys. Rev. B* **50**, 17953-17979

- (1994).
43. H. J. Monkhorst, J. D. Pack, Special points for Brillouin-zone integrations. *Phys. Rev. B* **13**, 5188-5192 (1976).
  44. M. Sakurai, J. R. Chelikowsky, Real-space pseudopotential method for calculating magnetocrystalline anisotropy. *Phys. Rev. Mater.* **2**, 084411 (2018).
  45. P. Giannozzi, S. Baroni, N. Bonini, M. Calandra, R. Car, C. Cavazzoni, D. Ceresoli, G. L Chiarotti, M. Cococcioni, I. Dabo, *et al.*, QUANTUM ESPRESSO: a modular and open-source software project for quantum simulations of materials. *J. Phys. : Condens. Matter* **21**, 395502 (2009).
  46. S. Q. Wu, M. Ji, C.-Z. Wang, M. C. Nguyen, X. Zhao, K. Umemoto, R. M. Wentzcovitch, K.-M. Ho, An adaptive genetic algorithm for crystal structure prediction. *J. Phys. : Condens. Matter* **26**, 035402 (2013).
  47. X. Zhao, M. C. Nguyen, W. Y. Zhang, C. Z. Wang, M. J. Kramer, D. J. Sellmyer, X. Z. Li, F. Zhang, L. Q. Ke, V. P. Antropov, K. M. Ho, Exploring the Structural Complexity of Intermetallic Compounds by an Adaptive Genetic Algorithm. *Phys. Rev. Lett.* **112**, 045502 (2014).
  48. M. S. Daw, M. I. Baskes, Semiempirical, Quantum Mechanical Calculation of Hydrogen Embrittlement in Metals. *Phys. Rev. Lett.* **50**, 1285-1288 (1983).
  49. G. Kresse, J. Furthmüller, Efficient iterative schemes for ab initio total-energy calculations using a plane-wave basis set. *Phys. Rev. B* **54**, 11169-11186 (1996).
  50. G. Kresse, J. Furthmüller, Efficiency of ab-initio total energy calculations for metals and semiconductors using a plane-wave basis set. *Comput. Mater. Sci.* **6**, 15-50 (1996).
  51. S. Steiner, S. Khmelevskiy, M. Marsmann, G. Kresse, Calculation of the magnetic anisotropy with projected-augmented-wave methodology and the case study of disordered Fe<sub>1-x</sub>Co<sub>x</sub> alloys. *Phys. Rev. B* **93**, 224425 (2016).
  52. H. Akai, P. H. Dederichs, A simple improved iteration scheme for electronic structure calculations. *Journal of Physics C: Solid State Physics* **18**, 2455-2460 (1985).
  53. M. Ogura, H. Akai, The full potential Korringa–Kohn–Rostoker method and its application in electric field gradient calculations. *J. Phys. Condens. Matter* **17**, 5741-5755 (2005).
  54. A. Togo, I. Tanaka, First principles phonon calculations in materials science. *Scr. Mater.* **108**, 1-5 (2015)
  55. A. Togo, First-principles Phonon Calculations with Phonopy and Phono3py. *J. Phys. Soc. Jpn.*, **92**, 012001-1-21 (2023)
  56. I. Levin (2018) NIST Inorganic Crystal Structure Database (ICSD).
  57. See Supplemental Material at [URL will be inserted by publisher] for structure information of the candidates and for AFM spin configurations examined.